

## Disulfide Bond Bridge Insertion Turns Hydrophobic Anticancer Prodrugs into Self-Assembled Nanomedicines

Yongjun Wang,<sup>\*,‡,○</sup> Dan Liu,<sup>§,○</sup> Qingchuan Zheng,<sup>||</sup> Qiang Zhao,<sup>†</sup> Hongjuan Zhang,<sup>¶</sup> Yan Ma,<sup>#</sup> John K. Fallon,<sup>†</sup> Qiang Fu,<sup>‡</sup> Matthew T. Haynes,<sup>†</sup> Guimei Lin,<sup>†</sup> Rong Zhang,<sup>△</sup> Dun Wang,<sup>§</sup> Xinggang Yang,<sup>‡</sup> Linxiang Zhao,<sup>§</sup> Zhonggui He,<sup>\*,‡</sup> and Feng Liu<sup>†,∞</sup>

<sup>†</sup>Division of Molecular Pharmaceutics, Eshelman School of Pharmacy, University of North Carolina at Chapel Hill, Chapel Hill, North Carolina 27599, United States

<sup>‡</sup>School of Pharmacy and <sup>§</sup>Key Laboratory of Structure-Based Drug Design and Discovery, Ministry of Education, Shenyang Pharmaceutical University, Shenyang 110016, China

<sup>||</sup>State Key Laboratory of Theoretical & Computational Chemistry, Institute of Theoretical Chemistry, Jilin University, Changchun 130012, China

<sup>†</sup>School of Chemical Engineering, Sichuan University, Chengdu 610065, China

<sup>¶</sup>Department of Medicinal Chemistry, School of Pharmacy, Nanjing Medical University, Nanjing 210029, China

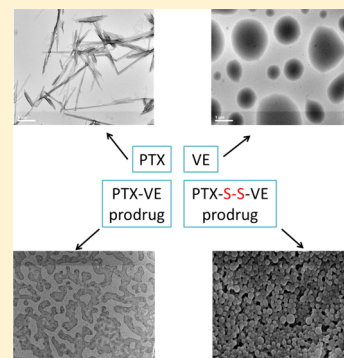
<sup>#</sup>School of Chinese Materia Medica, Guangzhou University of Chinese Medicine, Guangzhou 510405, China

<sup>†</sup>School of Pharmacy, Shandong University, Jinan 250012, China

<sup>△</sup>School of Pharmacy, Guangdong Pharmaceutical University, Guangzhou 510006, China

### Supporting Information

**ABSTRACT:** It is commonly observed that hydrophobic molecules alone cannot self-assemble into stable nanoparticles, requiring amphiphilic or ionic materials to support nanoparticle stability and function *in vivo*. We report herein newly self-assembled nanomedicines through entirely different mechanisms. We present proof-of-concept methodology and results in support of our hypothesis that disulfide-induced nanomedicines (DSINMs) are promoted and stabilized by the insertion of a single disulfide bond into hydrophobic molecules, in order to balance the competition between intermolecular forces involved in the self-assembly of nanomedicines. This hypothesis has been explored through diverse synthetic compounds, which include four first-line chemotherapy drugs (paclitaxel, doxorubicin, fluorouracil, and gemcitabine), two small-molecule natural products and their derivatives, as well as a fluorescent probe. Such an unprecedented and highly reproducible system has the potential to serve as a synthetic platform for a wide array of safe and effective therapeutic and diagnostic nanomedicine strategies.



**KEYWORDS:** nanomaterials, nanomedicines, nanoparticles, self-assemble, prodrug, disulfide bond

The field of nanomedicine is developing worldwide and is expected to bring radical solutions to many of modern medicine's limitations in drug delivery. The main challenges in nanomedicine involve efforts to improve cargo loading efficiency, pharmacokinetics (PK), therapeutic efficacy, live imaging, and ultimately clinical translation. Self-assembly of nanomaterials provides an attractive means by which to precisely engineer nanomedicines with distinct biophysical-chemical properties, thus simplifying the optimization of formulation.<sup>1,2</sup> At the molecular level, self-assembly involves competition between intermolecular (or thermodynamic) forces.<sup>3</sup> The forces are mainly van der Waals attraction and electrostatic repulsion, the former motivating agglomeration in order to minimize the free energy of the system, and the latter stabilizing nanoparticles (NPs) by repulsion of surrounding NPs. When these forces balance, agglomeration stops such that NPs are successfully self-assembled.<sup>3</sup> Force balancing relies

solely on either amphiphilic structures or ionic interactions with drugs. Hydrophobic drugs can self-assemble into NPs by either formation of micelles with amphiphilic surfactant molecules or by structure modification as amphiphilic prodrugs (e.g., conjugates to PEG, dendrimers, polypeptides, hydrogels).<sup>4–10</sup> Ionic drugs, on the other hand, can be coupled on the surface of oppositely charged colloidal particles, ultimately resulting in multilayered polyelectrolyte self-assembly.<sup>11–13</sup> However, as such systems present a variety of challenges in development, including formulation stability as well as drug loading and release, the generation of new nanomaterials with self-balancing

**Received:** June 1, 2014

**Revised:** August 30, 2014

**Published:** September 4, 2014

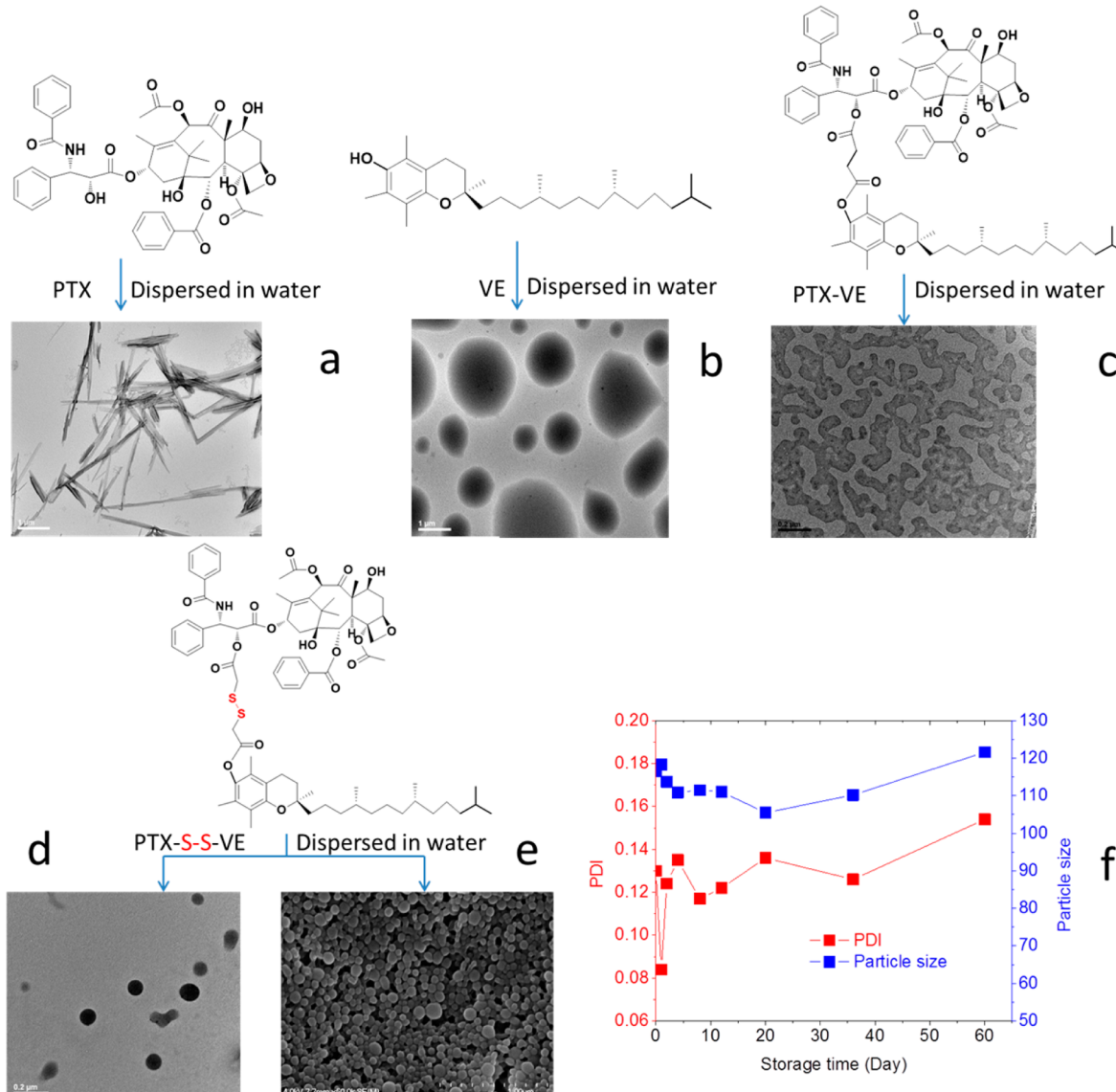


**Figure 1.** Characterization of various hydrophobic drugs dispersed in water. (a–c) Molecular structures of PTX, VE and PTX–VE and TEM images after dispersion in water. The sample in (b) (VE) was stained on the TEM grid immediately after the self-assembling process. Molecular structure of PTX–S–S–VE and TEM (d) and SEM (e) image of PTX–S–S–VE DSINMs. (f) Particle size distribution of PTX–S–S–VE DSINMs in DI water stored at 4 °C for two months. Scale bar: (a–b), 1 μm; (c–d), 0.2 μm; (e), 100 nm.

intermolecular force properties may be able to overcome the limitations of more conventional methods.

We report herein new nanomaterials composed of hydrophobic prodrugs that self-assemble into NPs by means independent of traditional amphiphilic or ionic interactions. Self-balancing intermolecular forces have been established by simple insertion of a disulfide bond between (1) two hydrophobic drugs, paclitaxel (PTX) or doxorubicin (DOX), and vitamin E (VE), (2) hydrophilic drugs fluorouracil (5-FU) or gemcitabine (GEM) and hydrophobic stearic acid (SA), and (3) a water-soluble fluorescent probe, sulforhodamine B (SRB), and VE. The synthesized molecules self-assemble into stable disulfide-induced nanomedicines (DSINMs) in aqueous suspension. In addition, we have synthesized two natural anticancer molecules and their derivatives, each of which contains a disulfide bond, and examined how their structures affect self-assembly.

We also present proof-of-concept methodology and results in support of our hypothesis that DSINMs are promoted and stabilized by the insertion of a disulfide bond to balance intermolecular forces. The structures and dynamic properties of the DSINMs at the molecular level have been explored, as have the mechanisms by which S–S bonds support the self-assembly and stabilization of the DSINMs. The PK, anticancer activity and tumor imaging of the DSINMs *in vitro* and *in vivo* have also been characterized, highlighting the strong potential of our synthetic platform in diverse nanomedical applications.

It is commonly understood that hydrophobic molecules alone cannot self-assemble into NPs. PTX and VE represent common molecules that, upon aqueous exposure, form large crystals or droplets (Figure 1a and b). When PTX is conjugated with VE as a prodrug (PTX–VE, Supporting Information Scheme S1), the hydrophobicity of the product is further increased, resulting in considerable aggregation during self-assembly (Figure 1c). Our data, however, shows that a single

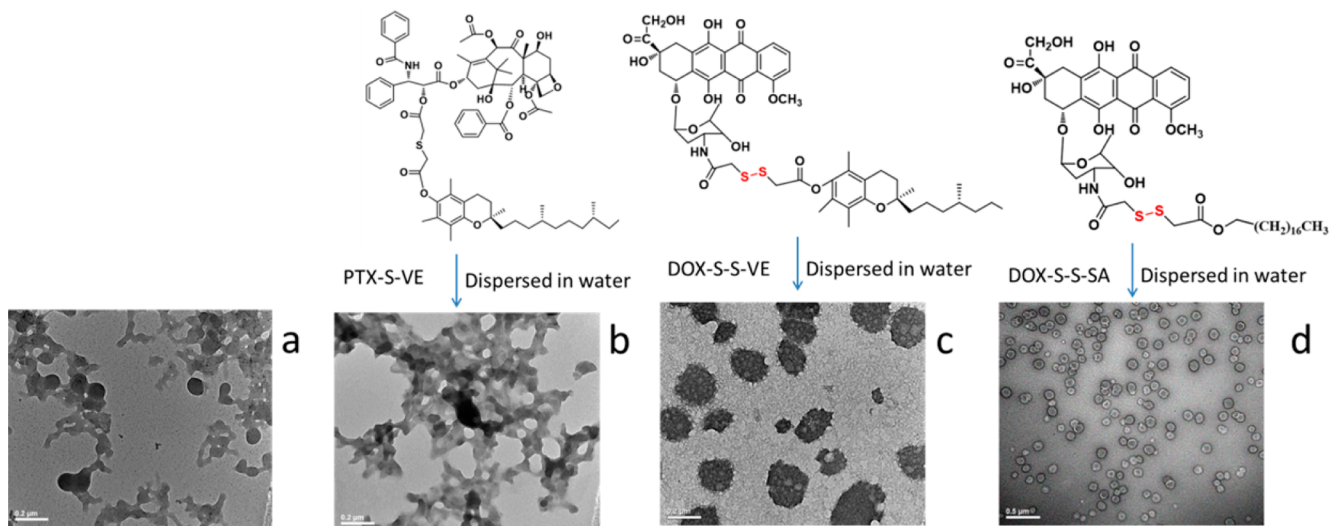


**Figure 2.** Illustration of the role of disulfide bond in self-assembly of DSINMs. (a) TEM image of PTX-S-S-VE DSINMs after incubation in 2.5 mM GSH for 0.5 h. (b) Molecular structure of PTX-S-VE and TEM image of PTX-S-VE after dispersion in water. (c–d) Molecular structures of DOX-S-S-VE and DOX-S-S-SA and TEM images of DOX-S-S-VE and DOX-S-S-SA DSINMs. Scale bar: (a–c), 0.2  $\mu$ m; (d), 0.5  $\mu$ m.

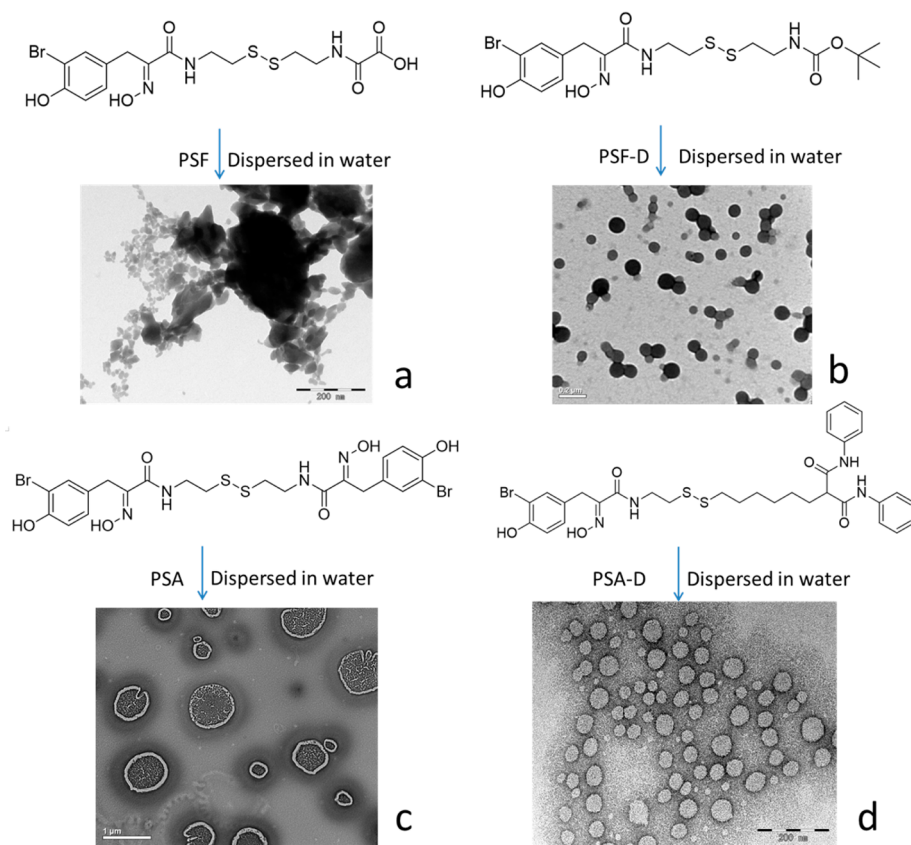


**Figure 3.** Molecular structures and TEM images of natural histone deacetylase inhibitors (HDACIs) and their derivatives after dispersion in water. (a) PSF, (b) PSF-D, (c) PSA, (d) PSA-D. Scale bar: (a–b), 0.2  $\mu$ m; (c), 1  $\mu$ m; (d), 0.2  $\mu$ m.

disulfide-bond inserted between the compounds (Figure 1d and e and Supporting Information Scheme S2 for synthesis) does not alter the hydrophobicity of the prodrug (Supporting Information Figure S1) but transforms its properties in aqueous suspension such that the self-assembled DSINMs are formed by prodrug alone (Figure 1e). The mean diameter of PTX-S-S-VE DSINMs was found to be  $113 \pm 5$  nm ( $n = 3$ ) with a unimodal size distribution ( $PDI < 0.16$ ) as measured by quasi-

elastic light scattering (Supporting Information Figure S2). The DSINMs exhibited excellent storage stability, with no significant change in the size over two months at 4 °C (Figure 1f). Such colloidal stability could be inferred by the particles' negative  $\zeta$  potential ( $\zeta$  potential = -29.2 mV). From the respective contributions of the molecular weights of PTX and VE in the conjugate, it was possible to calculate that the parent drug (PTX) loading was as high as 60 wt %, considerably

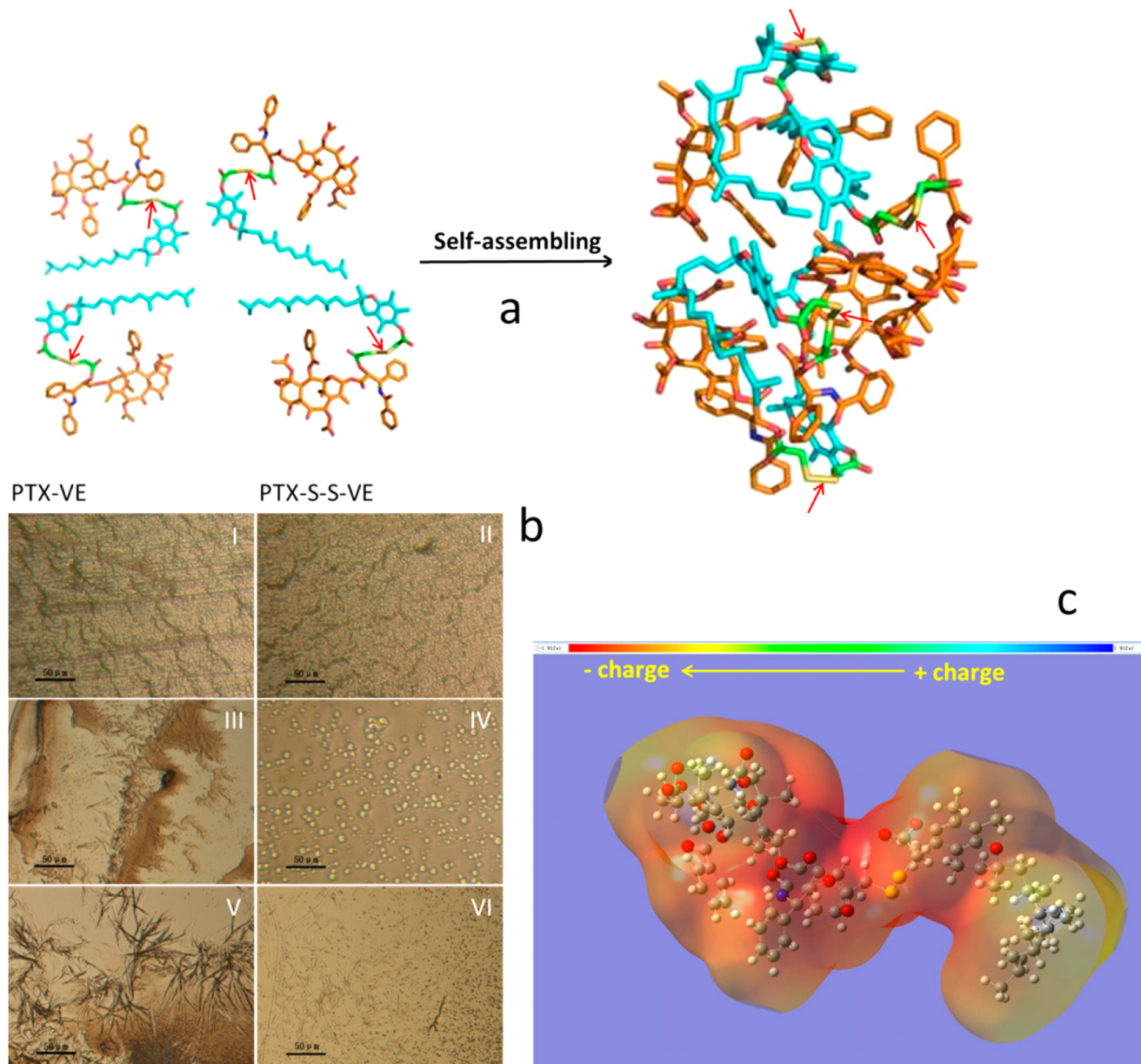


**Figure 4.** Characterization of the structure and formation of DSINMs. (a) MD simulations of tetrameric PTX–S–S–VE in water. The carbons are colored according to their molecule of origin: blue (VE), orange (PTX), and yellow (S–S). (b) Imaging the dynamics of crystal growth. Ethanol containing PTX–VE and PTX–S–S–VE was placed onto a glass slide. After drying and desiccating, a drop of water was added to each sample, the slides were placed into a humidified chamber at room temperature for various hydration times and pictures were taken. The left panel (I, III, and V) shows PTX–VE and the right panel (II, IV, and VI) PTX–S–S–VE. (c) The electrostatic potential map of PTX–S–S–VE.

higher than that of current commercially available dosage forms of PTX such as Taxol (1%) and Abraxane (10%).

Our initial expectation in exploring further the DSINM formulation was that the disulfide bond represents a key structure for self-assembly and stability. Indeed, successful glutathione (GSH) mediated reduction of the disulfide linkages in PTX–S–S–VE DSINMs caused the DSINMs to precipitate (Figure 2a), indicating that the architectural structures of the DSINMs are stabilized by the intact S–S. Agglomeration had also been observed (Figure 2b) in our attempts to formulate thioether-conjugated prodrugs into nanoparticles (PTX–S–VE, Supporting Information Scheme S3). In addition to the S–S moiety, we considered that VE or PTX may also be inherently responsible for the DSINM formation. Both the prodrug DOX–S–S–VE (Supporting Information Scheme S4) and the

prodrug DOX–S–S–SA (Supporting Information Scheme S5) were able to self-assemble into DSINMs with unimodal size distribution (Figure 2c and d and Supporting Information Figure S2). Disulfide bonds are fairly stable in normal biological conditions but are rapidly cleaved through thiol–disulfide exchange reactions facilitated by intracellular reducing molecules, especially GSH. It has been demonstrated that GSH concentrations in tumor cells (2–8 mM) are much higher than in blood plasma (1–2 μM).<sup>13,14</sup> Our data showed that the cleavage of S–S in PTX–S–S–VE by GSH results in the formation of PTX–SH, a less sterically hindered and more polar molecule. The hydrolysis rate of PTX–S–S–VE in the presence of GSH is far greater than that of PTX–VE (76% of PTX was released from PTX–S–S–VE vs <1% from PTX–VE after 24 h in PBS containing 1.0 mM GSH) (data not

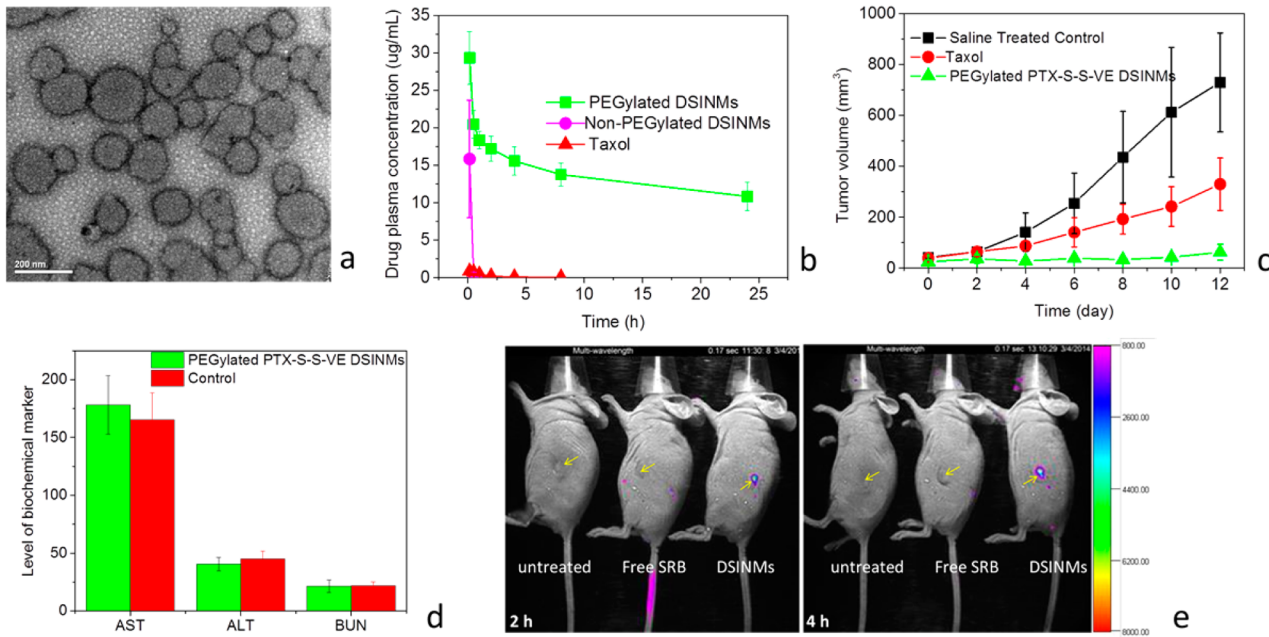


**Figure 5.** Characterization of PEGylated DSINMs for their physical image, plasma concentrations, anticancer activity, toxicity and tumor imaging. (a) TEM image of PTX-S-S-VE DSINMs PEGylated with 15% (w/w) DSPE-PEG2000. (b) Plasma concentration profiles of PEGylated and non-PEGylated PTX-S-S-VE DSINMs compared with Taxol ( $n = 3$ ). (c) Antitumor effects in mice models, \*\* $p < 0.01$  (Student's  $t$ -test, paired, two sided), compared with Taxol group and saline group ( $n = 5$ ). (d) Kidney and liver function parameters in PEGylated PTX-S-S-VE DSINM and saline treated control groups ( $n = 5$ ). (e) Tumor imaging in live mice. The tumor (indicated by arrows) bearing mice were imaged 2 and 4 h after injection of free SRB and PEGylated SRB-S-S-VE DSINMs. Images at 8, 12, and 48 h are shown in Supporting Information Figure S9.

shown). This indicates another advantage that DSINMs may offer for the enhanced delivery of anticancer drugs. Additionally, DSINMs are capable of delivering combined drugs (Supporting Information Figures S3 and S4).

Disulfide bonds are found in many small molecule natural products,<sup>14,15</sup> such as psammaplin F (PSF) and psammaplin A (PSA) isolated from the sponge *Pseudoceratina purpurea*. PSF and PSA exert anticancer activity through inhibition of both histone deacetylase (HDAC) and DNA methyltransferase.<sup>16</sup> We synthesized these two natural molecules and their derivatives (Figure 3 and Supporting Information Schemes S6 to S8) to evaluate whether they would self-assemble into DSINMs. The synthesized compounds showed similar anticancer cell and HDAC activities (Supporting Information Table S1). As shown in Figure 3a, PSF failed to form DSINMs, possibly because of its strongly polar carboxyl group. This was verified by synthesizing a derivative called PSF-D, in which the carboxyl group was replaced by a weakly polar group, *t*-butyloxycarbonyl. This derivative compound successfully self-assembled into DSINMs (Figure 3b, Supporting Information Figure S2). PSA, on the other hand, was able to self-assemble into DSINMs (Figure 3c), but its size (>400 nm, Supporting Information Figure S2) was bigger than that of PSF-D. The increased size may have been due to the polarity of two substituted phenylalanine (PHE) amides linked to both sides of the S-S (though not as strongly as the carboxyl group for PSF). Therefore, we synthesized a PSA derivative (PSA-D) in which one PHE amide was substituted with a low-polar moiety di(phenylaminocarbonyl) group, resulting in the formation of DSINMs of 90 nm in size (Figure 3d and Supporting Information Figure S2). All of this data suggests that the polarity of moieties that flank S-S also play an important role in the self-assembly of DSINMs.

To explore the self-assembling behavior of the DSINMs, molecular dynamics (MD) simulations for the tetramer PTX-S-S-VE were performed. The final MD simulation position after 10 ns in water is shown in Figure 4a (right side). Molecules were initially arranged approximately 10 Å apart (left panel) to support an unmanipulated assembly process. Our data indicated that four molecules quickly came together to form a cluster of tetramers. As soon as the self-assembly was completed, the conformation did not change much. Only movement of the whole cluster was observed. As shown in Figure 4a, the long alkyl chains of VE are curved inside the cluster and there are no direct interactions between S-S bonds (indicated by arrows). Considering the structure of the tetramer, we can assume that the driving forces for the self-assembly of the DSINMs are nonbonded hydrophobic interactions, with PTX interacting with PTX, PTX with VE, or VE with VE. However, when the S-S bonds are broken, more energetically favorable conformations may be possible between components, disrupting the DSINM structure.

PTX-VE, which contains no S-S linkage, fails to form NPs through a self-assembly process, instead forming crystal aggregates. It is known that crystal growth yields an ordered and repeating pattern of atoms or molecules extending in all three spatial dimensions, precipitating product from solution in favor of solvent–solvent interactions. For self-assembly of NPs, such a thermodynamically favored process needs to be abrogated and assembled structures forced to interact in a direct way with the solution phase. Structural interactions observed in the MD simulations suggest that self-assembly of DSINMs may be supported through a hindrance of crystallization due to inclusion of the disulfide bond. To explore this concept further, we examined the crystallization kinetics of PTX-VE and PTX-S-S-VE by imaging. As shown in Figure 4b-I and II, both PTX-VE and PTX-S-S-VE

formed amorphous precipitate after ethanol evaporation. Two hours after hydration, crystals were observed for PTX–VE (Figure 4b-III). In contrast, no crystals were detected for PTX–S–S–VE. Instead, the hydration induced spherical particles of diameter  $<10\text{ }\mu\text{m}$  (Figure 4b-IV). At longer hydration times ( $\sim 12\text{ h}$ ), larger crystals were formed for PTX–VE (Figure 4b-V), whereas small crystals were observed in the PTX–S–S–VE sample (Figure 4b-VI). Thus, we can infer that simple insertion of S–S in the prodrugs serves in part to inhibit crystallization and drive the prodrugs instead toward the formation of nanoparticles.

The  $\zeta$  potential data showed the surface charge of the DSINMs to be  $-20$  to  $-30\text{ mV}$ , an important property stabilizing the particles. Considering the MD analysis already shown, one would expect the PTX portion of PTX–S–S–VE, which contains some polar moieties (e.g., OH or C=O), to expose itself at the surface of particles in order to stabilize the particle–solution interface. We next tested how the S–S moiety contributes to the charge. The calculation of the charge density in aqueous solution was based on the self-consistent reaction field (SCRF) method with the polarizable continuum model (PCM).<sup>17,18</sup> It was done using the GAUSSIAN 03 program and optimized using the PM3 method. As shown in Figure 4c, PTX (left portion) is the major negatively charged donor. VE (right portion) and the two sulfur atoms (central portion) do not contribute to the negative charge. However, a negative charge coming mainly from oxygen is concentrated near the S–S bond. It is well known that S–S bonds show a distinct preference for dihedral angles approaching  $90^\circ$ . This may play an essential role in balancing intermolecular forces and establishing a favorable conformation, that is, exposing the high density of negative charge on the DSINMs surface and contributing to the overall disruption of crystal formation.

PEGylation of NPs provides an effective means to reduce clearance by the reticuloendothelial system (RES).<sup>19</sup> We, therefore, PEGylated DSINMs by mixing 15% (w/w) DSPE-PEG2000 with PTX–S–S–VE DSINMs. TEM images clearly confirmed PEGylation of DSINMs (Figure 5a). The particle size of PEGylated DSINMs was 124.9 nm (Supporting Information Figure S2, last image), and  $\zeta$  potential was  $-28.7\text{ mV}$ . To evaluate the behavior of the DSINMs in mice, the PTX–S–S–VE DSINMs with and without PEGylation were administered systemically. Plasma concentration of PTX–S–S–VE was measured as a function of time postinjection. The data was fitted to a noncompartmental pharmacokinetic model (Figure 5b and Supporting Information Table S2). Non-PEGylated DSINMs and Taxol were cleared rapidly from the blood. However, the circulation time of PEGylated DSINMs was greatly improved, yielding a terminal half-life ( $t_{1/2}$ ) of  $25.74 \pm 7.66\text{ h}$  compared to a  $t_{1/2}$  of  $1.47 \pm 0.16\text{ h}$  ( $p < 0.05$ , Student's  $t$ -test, paired, two sided) for Taxol. The  $AUC_{0-t}$  values of PEGylated PTX–S–S–VE DSINMs were 250-fold higher than those of Taxol ( $p < 0.01$ , Student's  $t$ -test, paired, two sided). Altered biodistribution profiles of PEGylated DOX–S–S–SA DSINMs provide additional information that PEGylation can improve the blood retention of DSINMs (Supporting Information Figure S5). All these results suggested that the PEGylated DSINMs may be likely to preferentially accumulate in solid tumors to a greater extent than Taxol via the enhanced permeability and retention (EPR) effect.

To evaluate the *in vivo* antitumor efficacy, human epidermoid carcinoma cell line KB-3-1 tumor bearing mice were IV injected with PEGylated PTX–S–S–VE DSINMs or

Taxol at PTX equivalent doses of  $5\text{ mg/kg}$  every second day, starting 6 days after inoculation (when tumor diameter was  $4\text{--}6\text{ mm}$ ). Compared with Taxol, PEGylated PTX–S–S–VE DSINMs showed significant inhibition of the KB-3-1 tumors (Figure 5c,  $p < 0.01$ , Student's  $t$ -test, paired, two sided). This significantly improved *in vivo* efficacy could be attributed to the enhanced PTX–S–S–VE PK profiles mentioned above that would result in greater accumulation of drug at the tumor site. No weight loss occurred in the mice treated with the PEGylated PTX–S–S–VE DSINMs (Supporting Information Figure S6), demonstrating the tolerability of the particles.

In order to determine the safety of the PTX–S–S–VE DSINMs for IV administration, the hemolytic potential of the formulation was evaluated (Supporting Information Figure S7). Levels of serum aspartate transaminase (AST), alanine transaminase (ALT), and blood urea nitrogen (BUN) were also examined to explore hepatic and renal toxicity. After mice ( $n = 5$ ) were successively administrated PEGylated PTX–S–S–VE DSINMs daily for 5 days at PTX equivalent doses of  $10\text{ mg/kg}$ , the ALT, AST, and BUN levels were not significantly different from those in the saline treated control group (Figure 5d). Taking the hemolytic test and liver and kidney function tests together, the PTX–S–S–VE DSINMs exhibited good safety.

The DSINMs ability to carry water-soluble drugs 5-FU and GEM encouraged us to explore whether they could also carry a water-soluble fluorescent probe, namely sulforhodamine B (SRB), for tumor imaging. Both SRB–VE and SRB–S–S–VE were synthesized (Supporting Information Scheme S9). Again, a single S–S insertion turned what would otherwise form large aggregates (SRB–VE) into DSINMs (Supporting Information Figure S8, SRB–S–S–VE). Tumor imaging was performed for free SRB and PEGylated SRB–S–S–VE DSINMs, after injection into tumor bearing mice. Whole body imaging showed that no fluorescence signal was detectable in the tumors in the mice injected with free SRB throughout the entire imaging process. However, for the PEGylated DSINMs, the fluorescence signal was detected from the tumor at  $2\text{ h}$  (Figure 5e) and reached a maximum level between  $4$  and  $8\text{ h}$  after injection. It then decreased until no signal was detectable  $2\text{ days}$  after injection (Supporting Information Figure S9). Therefore, it is expected that PEGylated DSINMs, when carrying fluorophores, may represent a promising theranostic tool for tumor imaging.

DSINMs show strong potential for use as an entirely new nanomedicine platform for self-assembly of NPs in drug delivery and imaging. The inserted S–S bond plays a unique role in balancing the intermolecular forces that control the self-assembly of the NPs. Our MD simulation results support the view that dihedral angles of  $90^\circ$  are generated at the disulfide linkage during the self-assembly process, generating a stable conformation of the prodrugs in a nonregular and nonperiodic manner (Figure 4a). Further analysis of the crystallization kinetics with and without the disulfide linkage suggests that S–S bonds abrogate crystal growth during self-assembly. In addition, the configuration of S–S bonds that are not sterically hindered and project from the cluster (Figure 4c) may contribute to the stabilization of the DSINMs by presenting a high density of negative charge (near the S–S bonds) at the surface.

PTX prodrug has been employed here as a model for the proof-of-concept studies of our DSINMs. A prodrug is a bioreversible derivative of an active drug, and it is commonly

included in drug design and development. As many as 14% of all new approved drugs worldwide can be classified as prodrugs.<sup>20</sup> Many efforts have been made to develop PTX prodrugs,<sup>21,22</sup> and nanoformulations such as Taxol and Abraxane have been developed. Toxicity and the short  $t_{1/2}$  of PTX are problems with the use of Taxol.<sup>23,24</sup> Although Abraxane has been shown to have several practical advantages over Taxol, it does not significantly improve the PK or biodistribution (BD) of the PTX.<sup>25,26</sup> As shown in Figure 5b to d and Supporting Information Figures S5 and S7 and Table S2, DSINMs present markedly reduced toxicity by comparison and show significant improvement in PK and therapeutic efficacy.

The increased number of poorly soluble compounds in drug development has become an industry wide concern for which the development of advanced delivery systems has predominated as a potential solution.<sup>27</sup> DSINM technology expands formulation development potential by utilizing novel synthetic chemistry in the physical self-assembly process, presenting opportunities for the development of novel nanocarriers with improved loading and stability while remaining amenable to modification and coformulation with traditional materials. DSINMs have been successfully tested with four first line chemotherapy drugs (PTX, DOX, 5-FU, and GEM), two anticancer molecules of natural origin, and a fluorescent probe for live animal tumor imaging. We believe that DSINMs can be used to promote the screening of a wide library of small molecules with promising anticancer properties for clinical translation.

In summary, our data has shown that insertion of a single disulfide bond can transform hydrophobic prodrugs and imaging probe into suitable nanomaterials for molecular self-assembly independent of excipients. Such reliable self-assembly dramatically increases drug loading and alleviates concerns over excipient associated adverse effects. The PEGylated DSINMs have shown both improved PK and anticancer efficacy over traditional PTX formulations, with suitable tumor imaging capability. The DSINM technology, which has not been previously demonstrated, is shown to be highly reproducible and should motivate the development of new nanomedicines for drug delivery and imaging.

## ■ ASSOCIATED CONTENT

### Supporting Information

Preparation and characterization of DSINMs; separation of DSINMs by sucrose density gradient centrifugation; HDACs inhibition and cytotoxicity assays; molecular dynamics simulations; in vivo antitumor and imaging studies; synthesis of diverse compounds; additional measurements and imaging. This material is available free of charge via the Internet at <http://pubs.acs.org>.

## ■ AUTHOR INFORMATION

### Corresponding Authors

\*E-mail: (Y.W.) wangyjspu@163.com.

\*E-mail: (Z.H.) hezhonggui@vip.163.com.

### Author Contributions

○Both contributed to this work equally.

### Notes

The authors declare no competing financial interest.

<sup>∞</sup>Deceased

## ■ ACKNOWLEDGMENTS

This work was supported by the National Cancer Institute—National Institutes of Health (5R01CA149387).

## ■ DEDICATION

Dedicated to the memory of Professor Feng Liu, Ph.D., 1955–2014, University of North Carolina at Chapel Hill.

## ■ REFERENCES

- (1) Shi, J.; Votruba, A. R.; Farokhzad, O. C.; Langer, R. *Nano Lett.* **2010**, *10*, 3223–3230.
- (2) Han, W.; Lin, Z. *Angew. Chem., Int. Ed.* **2012**, *51*, 1534–46.
- (3) Clancy, P. *Nat. Nanotechnol.* **2011**, *6*, 540–1.
- (4) Bolton, J.; Bailey, T. S.; Rzayev, J. *Nano Lett.* **2011**, *11*, 998–1001.
- (5) Ernsting, M. J.; Tang, W. L.; MacCallum, N. W.; Li, S. D. *Biomaterials* **2012**, *33*, 1445–54.
- (6) Williams, S. R.; Lepene, B. S.; Thatcher, C. D.; Long, T. E. *Biomacromolecules* **2009**, *10*, 155–61.
- (7) MacKay, J. A.; Chen, M.; McDaniel, J. R.; Liu, W.; Simnick, A. J.; Chilkoti, A. *Nat. Mater.* **2009**, *8*, 993–9.
- (8) Joralemon, M. J.; McRae, S.; Emrick, T. *Chem. Commun.* **2010**, *46*, 1377–93.
- (9) Gaucher, G.; Marchessault, R. H.; Leroux, J. C. *J. Controlled Release* **2010**, *143*, 2–12.
- (10) Vemula, P. K.; Wiradharma, N.; Ankrum, J. A.; Miranda, O. R.; John, G.; Karp, J. M. *Curr. Opin. Biotechnol.* **2013**, *24*, 1174–82.
- (11) Schiffrin, A.; Riemann, A.; Auwarter, W.; Pennec, Y.; Weber-Bargioni, A.; Cvetko, D.; Cossaro, A.; Morgante, A.; Barth, J. V. *Proc. Natl. Acad. Sci. U.S.A.* **2007**, *104*, 5279–84.
- (12) Bhosale, S. V.; Kalyankar, M. B.; Nalage, S. V.; Lalander, C. H.; Langford, S. J.; Oliver, R. F. *Int. J. Mol. Sci.* **2011**, *12*, 1464–73.
- (13) Ipe, B. I.; Mahima, S.; Thomas, K. G. *J. Am. Chem. Soc.* **2003**, *125*, 7174–5.
- (14) Wang, C.; Wesener, S. R.; Zhang, H.; Cheng, Y.-Q. *Chem. Biol.* **2009**, *16*, 585–593.
- (15) Jacob, C. *Nat. Prod. Rep.* **2006**, *23*, 851–63.
- (16) Pina, I. C.; Gautschi, J. T.; Wang, G. Y.; Sanders, M. L.; Schmitz, F. J.; France, D.; Cornell-Kennon, S.; Sambucetti, L. C.; Remiszewski, S. W.; Perez, L. B.; Bair, K. W.; Crews, P. *J. Organomet. Chem.* **2003**, *68*, 3866–73.
- (17) Caricato, M.; Scalmani, G.; Trucks, G. W.; Frisch, M. J. *J. Phys. Chem. Lett.* **2010**, *1*, 2369–2373.
- (18) Liang, W.; Li, X.; Dalton, L. R.; Robinson, B. H.; Eichinger, B. E. *J. Phys. Chem. B* **2011**, *115*, 12566–70.
- (19) Jokerst, J. V.; Lobovkina, T.; Zare, R. N.; Gambhir, S. S. *Nanomed.* **2011**, *6*, 715–28.
- (20) Huttunen, K. M.; Rautio, J. *Curr. Top. Med. Chem.* **2011**, *11*, 2265–87.
- (21) Zhang, Z.; Mei, L.; Feng, S. S. *Expert Opin. Drug Delivery* **2013**, *10*, 325–40.
- (22) Skwarczynski, M.; Hayashi, Y.; Kiso, Y. *J. Med. Chem.* **2006**, *49*, 7253–69.
- (23) Steed, H.; Sawyer, M. B. *Pharmacogenomics* **2007**, *8*, 803–15.
- (24) Straub, J. A.; Chickering, D. E.; Lovely, J. C.; Zhang, H.; Shah, B.; Waud, W. R.; Bernstein, H. *Pharm. Res.* **2005**, *22*, 347–55.
- (25) Kamaly, N.; Xiao, Z.; Valencia, P. M.; Radovic-Moreno, A. F.; Farokhzad, O. C. *Chem. Soc. Rev.* **2012**, *41*, 2971–3010.
- (26) Scripture, C. D.; Figg, W. D.; Sparreboom, A. *Ther. Clin. Risk Manage.* **2005**, *1*, 107–14.
- (27) Mustelin, T. *Nanomed.* **2006**, *1*, 383–5.